2014 International Conference on Unmanned Aircraft Systems (ICUAS)
May 27-30, 2014. Orlando, FL, USA

Wind Tunnel Testing of a VTOL MAV Propeller in Tilted Operating Mode*

B. Theys, G. Dimitriadis, T. Andrianne, P. Hendrick and J. De Schutter

Abstract— **This paper presents experimental results of the full 3-axis force vector and 3-axis moment vector acting on a propeller, commonly used for a Vertical Take Off and Landing Micro Aerial Vehicle (VTOL MAV). Measurements were carried out in a wind tunnel using a high resolution 6-axis force/moment sensor embedded in a customized test rig at several wind speeds, propeller rotational speeds and angles of the propeller shaft with respect to the air stream. Results show strong moments acting on the propeller in forward flight and unstable conditions in descending flight. Power calculations reveal a decrease in power consumption during slow forward flight and how motor efficiency can be maximized.**

I. Introduction

Recent advances in sensing technology and data processing have led to great opportunities in design and development of autonomous MAVs for various applications such as monitoring, exploration and even transportation. Among these MAVs, VTOL MAVs prove to be advantageous for deployment in several autonomous applications, since they are capable of hovering, hence not require a runway. While a lot of research concerning these vehicles focusses on control near hover conditions, only little is known about flight performance at higher speeds.

Optimal design [1], modeling [2,3] and control of these vehicles requires detailed propeller performance data. For some propellers, these data are provided by the propeller manufacturer [4] after performing a classic wind tunnel test in which thrust and torque are measured at various propeller rotational speeds and wind speeds as in [5-10]. During these measurements, air flow is parallel to the propeller shaft as this is also the case for most airplanes for which wings provide lift and the propeller provides forward propulsion. VTOL MAVs, however, use their propellers both for forward propulsion and for lift to take off and land vertically. As a result, their propellers are often used in tilted operating mode throughout the flight envelope as illustrated in Fig.1. Only few data exist about small propellers in tilted operation [11-13]. Modeling these propellers is hard, since they operate at low Reynolds numbers [14], for which classical helicopter disk theory is no longer proven. Momentum and blade element theory used in these models would also require detailed information about propeller geometry and used airfoils, which are usually not provided by the propeller manufacturers. In a lot of studies, the propeller is therefore simply modeled in its hover regime, which is then used for the whole flight envelope [15,16]. This is justified because the VTOL MAV is only used in slow forward flight. For various applications however, MAVs have to operate outdoors at higher speeds, deviating significantly from the hover flight regime [17].

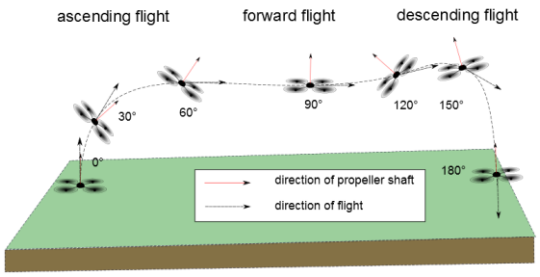

Figure 1. Different operating modes of a propeller throughout the flight of a VTOL MAV with their corresponding propeller angles.

II. Experimental Setup

The experiments are performed in the subsonic wind tunnel of the University of Liège (ULg), a detailed description of which can be found in [18]. The general specifications are presented in Table 1.

TABLE I. General specifications of the wind tunnel

Dimensions of test section	2m x 1.5m x 5m (width x height x length)
Speed range	2-60m/s
Test table	diam 1.5m, rotation ±90°
Speed non-uniformity	< 0.5%

*Research supported by FWO grant G.0404.10.

B. Theys is with the Department of Mechanical Engineering PMA, KU Leuven, Leuven, 3000 Belgium (phone: +32-16-328058; e-mail: bart.theys@kuleuven.be).

G. Dimitriadis is with the Department of Aerospace and Mechanical engineering, University of Liege, Liege, 4000 Belgium (e-mail: gdimitriadis@ulg.ac.be).

T. Andrianne is with the Department of Aerospace and Mechanical engineering, University of Liege, Liege, 4000 Belgium (e-mail: t.andrianne@ulg.ac.be).

P. Hendrick is with the Aero-Thermo-Mechanics Department – Fluid Mechanics Université Libre de Bruxelles, Brussels, 1000 Belgium (e-mail: patrick.hendrick@ulb.ac.be).

J. De Schutter is with the Department of Mechanical Engineering PMA, KU Leuven, Leuven, 3000 Belgium (e-mail: joris.deschutter@kuleuven.be).

Air speed is measured via a Pitot tube and data are collected, processed and displayed by a KIMO CP300 system. An overview of the test setup is given in Fig. 2. The propeller inside the wind tunnel is a Graupner E-prop 9x5, commonly used for multi-rotors. The propeller is driven by a brushless direct current (BLDC) motor controlled by an electronic speed controller (ESC). The speed of the motor is varied by either changing the voltage of the power supply or by limiting the throttle setting of the ESC. To reduce vibrations, the propeller is balanced using a prop balancer on which the propeller is magnetically suspended to eliminate friction. The heavier side of the propeller is sanded until it is in perfect balance. Precise balancing of the propeller proved to successfully reduce the amplitude of these vibrations. The motor is mounted on a 6-axis "ATI Nano 17" force/moment sensor [19]. The force/moment sensor can measure a thrust force ranging from $-17\,N$ up to $17\,N$ and force along the other axes from $-12\,N$ up to $12\,N$ with a resolution of $1/320\,N$. Moments on all axis can be measured ranging from $-0.12\,Nm$ to $0.12\,Nm$ with a resolution of $1/6400\,Nm$. A custom made nacelle produced by using rapid prototyping isolates the force/moment sensor and wiring of the motor from any disturbing aerodynamic forces (Fig. 3). The setup is powered by a DC power supply outside the wind tunnel. Current is measured at the power supply itself while the voltage is measured at the input of the ESC to exclude voltage losses in the cable between power supply and test rig. Propeller rotational speed is found by measuring pulses from one of the three wires of the BLDC motor, taking into account the 14 poles of the motor. This whole test rig (Fig. 4) is mounted on a turntable inside the wind tunnel, allowing it to turn over a range of $180\,°$. Table 2 presents an overview of the different components used for the experiment.

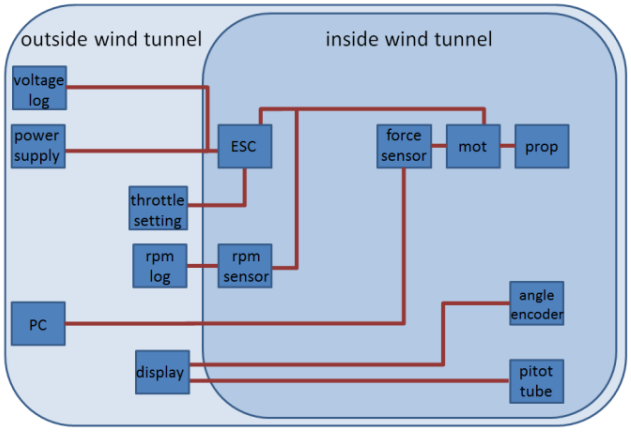

Figure 2. Overview of the different components used in the test setup.

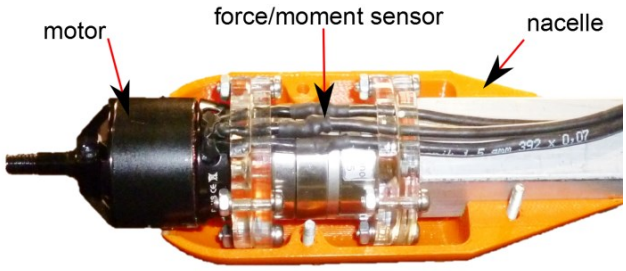

Figure 3. Assembly of the force/moment sensor inside the nacelle.

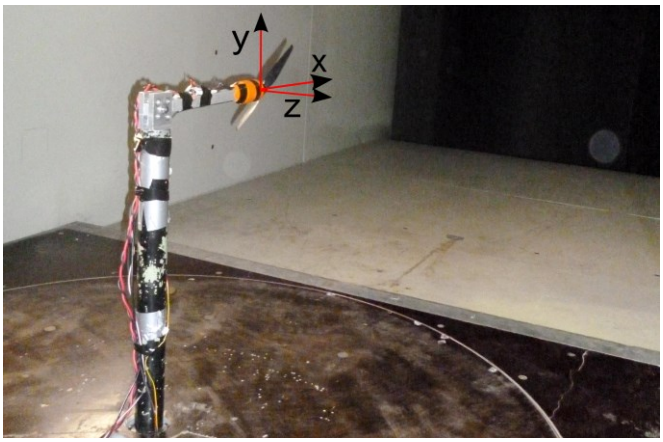

Figure 4. Test rig inside the wind tunnel.

TABLE II. LIST OF THE DIFFERENT COMPONENTS

DC power supply	Delta Elektronika SM 18 -50
ESC	DJI Innovations 30A
Motor	AscTec Pelican BLDC
Force/moment sensor	ATI Nano 17 – SI-12-0.12 calibrated
RPM senor	Eagle Tree brushless RPM sensor
Propeller	Graupner E-prop 23-12.5 (9x5)
Throttle set	Turnigy ccpm servo consistency master

III. EXPERIMENT

The forces and moments acting on a propeller are function of three parameters: wind speed, propeller angle and propeller rotational speed.

3.1. Conventions

In this paper the force and moment vector are represented following a commonly used convention for airplanes in which the x-axis lies in the extension of the motor axis and z- and y-axes lie on the propeller disk with z pointing down and y right. This convention is illustrated in Fig. 5. The propeller angle lies in the xz plane and is measured between the motor shaft (x-axis) and the air stream. The y-axis is always aligned with the height of the wind tunnel.

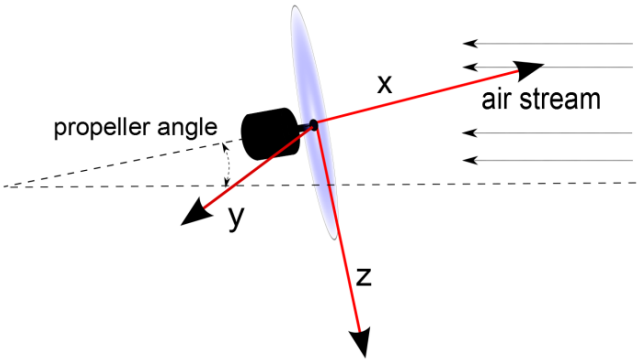

Figure 5. Convention of the propeller angle and the axes, attached to the propeller.

Air temperature and pressure are logged to calculate the air density. The dimensionless forces and moments on the propeller are calculated as:

$$C_{F_{[x,y,z]}} = \frac{F_{[x,y,z]}}{\rho n^2 D^4}, \qquad C_{M_{[x,y,z]}} = \frac{M_{[x,y,z]}}{\rho n^2 D^5}. \tag{1}$$

Here D is the diameter of the propeller, ρ the air density and n the number of revolutions per second. Note that these formulas are used for propellers: for a helicopter rotor, these coefficients are defined differently [20]. Table 3 presents an overview of the measured forces and moments with their corresponding dimensionless constants. For an airplane propeller, the moment M_z corresponds to the P-factor, producing a yawing moment and F_y and F_z are the y - and z - component of the propeller normal force. In addition, voltage and current are measured to calculate motor and speed controller efficiency.

$$\eta_{motor+esc} = \frac{2\,\pi\,n\,M_x}{U\,I} \tag{2}$$

U is the measured voltage [V] and I the measured current [A].

TABLE III. OVERVIEW OF THE FORCES AND MOMENTS WITH THEIR CORRESPONDING DIMENSIONLESS CONSTANTS

Dimensional		Dimensionless	
F_x	*thrust*	C_{F_x}	*thrust coefficient*
F_y	*y - hub force*	C_{F_y}	*y - hub force coefficient*
F_z	*z - hub force*	C_{F_z}	*z - hub force coefficient*
M_x	*torque*	C_{M_x}	*torque coefficient*
M_y	*pitching moment*	C_{M_y}	*pitching moment coefficient*
M_z	*yawing moment*	C_{M_z}	*yawing moment coefficient*

3.2. Coordinate Transformation

Since the force/moment sensor measures forces and moments in its own coordinate system, measurements have to be transformed to the propeller coordinate system. The force/moment sensor is mounted about $0.040\,m$ behind the propeller and small errors in the test rig assembly cause the force/moment sensor to not be perfectly aligned with the propeller. These translations and rotations between sensor and propeller are determined by performing three calibration experiments. In the first experiment a weight is suspended on the origin of the propeller coordinate system to apply a pure force in the z-direction. This experiment is repeated after turning the test rig 90° around the x-axis to obtain a force in the y-direction. In the last experiment, the propeller turns at zero wind speed, producing only a thrust and a torque in the propeller coordinate system.

3.3. Test Procedure

During the experiments the wind speed is held constant and a propeller angle is set. Three wind speeds are used: $0\,m/s$, $6\,m/s$ and $9\,m/s$. Propeller angles vary from 0° to 180°. In braking or descending flight, thrust counteracts the flight direction, represented by propeller angles between 90° and 180°. These conditions are characterized by unsteady flows in which theoretical approaches are usually invalid. Because little is known about these flight regimes, measurements include the full flight envelope from a propeller angle of 0° up to 180° as presented in Fig. 6.

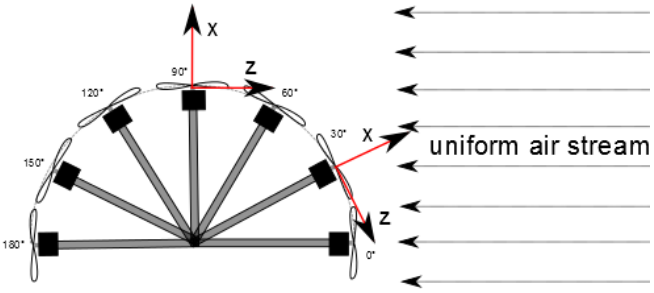

Figure 6. Different propeller angles during test procedure.

Measurements are recorded for several rotational speeds at constant wind speed and propeller angle. Therefore the input voltage of the motor, regulated by the power supply, is varied between $4V$ and $12V$, resulting in propeller rotational speeds from $3000\,rpm$ up to $10000\,rpm$. Note that the rotational speed can also be changed by the throttle setting of the ESC. A comparison between these two methods is made in section 4.5. Table 5 shows the different parameters used.

TABLE V. INDEPENDENTLY ADAPTABLE INPUT PARAMETERS RESULTING IN 135 DIFFERENT OPERATING MODES OF THE PROPELLER

Wind speed V	0 6 9	[m/s]
Propeller angle α_{prop}	0 30 60 90 120 150 180	[°]
Input voltage U	4 5 6 7 8 9 10 11 12	[V]

After obtaining a steady flow, measurements are recorded during 1 second at $2500Hz$, resulting in a Nyquist frequency of $1250\,Hz$, well above the maximum rotational speed of $10000\,rpm$ ($167\,Hz$). During the experiment the voltage is first increased in steps of $1\,V$ up to $12\,V$ and then back decreased to $4\,V$, resulting in two measurements for every voltage. This way hysteresis of the sensor can be accounted for.

IV. Results and Discussion

The propeller used during the experiments is designed to turn counterclockwise. For multi-rotor VTOL MAVs, usually both clockwise and counterclockwise propellers are used. In the case of a clockwise turning propeller F_y, M_x and M_z change sign.

Fig. 7 and 8 present respectively the resulting force and moment coefficients, acting on a propeller in tilted operation. These dimensionless coefficients are calculated following (1). Each graph contains one coefficient for a range of rotational speeds at a constant propeller angle for both $6\,m/s$ and $9\,m/s$ wind speed. Measurements of the propeller at $0\,m/s$ are added in the graphs only at $0°$ propeller angle. At 90° propeller angle there are no data for $9\,m/s$ wind speed due to sensor saturation. Also due to strong vibrations around $5000\,rpm$, several measurements are lacking.

4.1 Forces

The maximum measured thrust during the experiments is $8\,N$ or 47% of the sensor range. Fig. 7 shows the thrust coefficient in the first column. The two measured values for each applied voltage lie close to each other, only for the experiment at $0\,m/s$ little hysteresis of the sensor can be observed. At 0° propeller angle, the thrust coefficient decreases with an increase in wind speed as expected. This creates a stable ascending flight for a VTOL MAV in which a disturbance resulting in a higher climbing speed decreases thrust, hence reducing the climbing speed. This thrust difference between the two air speeds diminishes for higher propeller angles and disappears at 60°. At 90° and $6\,m/s$ the propeller produces more thrust than in the case of 0° and $6\,m/s$ and this difference is stronger at lower rpm. There is no noticeable difference in thrust compared to hover. Angles greater than 90° represent a VTOL MAV in descending flight. For 120° and 150° the increased thrust at higher air speed will result in a stable descending speed of the vehicle. However at 180° the thrust coefficient at higher rpm seems independent of the wind speed. This suggests that a descending flight can be unstable, since an increased descending speed does not result in a higher lifting force. In this regime, a vortex ring state may occur as described and tested in [23].

Forces in y and z direction occur if the propeller blades experience a different flow velocity throughout one revolution. The second and third column of Fig. 7 present the dimensionless hub force coefficients in y and z direction. These force coefficients are small compared to the thrust coefficient C_{F_x}. The maximum measured hub force is $0.4\,N$. This is 3.3% of the sensor range in these directions and 20 times smaller than the maximum measured thrust. Note that the scale of column 2 and 3 of Fig. 7 is smaller.

The force coefficient C_{F_y} at 0° is expected to be zero. The small offset that can be seen on the graph is likely to be caused by a small difference in mounting angle of the propeller onto the force/moment sensor compared to the calibration experiment. Because the hub forces are one or two orders of magnitude smaller compared to the thrust force, a small difference in alignment of the sensor with the propeller compared to the alignment during calibration causes the sensor to measure a part of the thrust as hub force. The force coefficient C_{F_y} stays very small for other propeller angles. The force coefficient C_{F_z} however, shows to be clearly negative between 30° and 150° propeller angle. This force represents a drag force, decreasing the speed of the VTOL MAV. This force becomes stronger at increased wind speed.

4.2 Moments

The maximum measured torque during the experiments is $0.1\,Nm$ or 83% of the sensor range. The first column of Fig. 8 shows the torque coefficient C_{M_x}. At angles between 60° and 180° the torque coefficient is not much affected by the propeller angle or wind speed. At small angles, the absolute value of the torque coefficient decreases at higher wind speeds and lower rpm. At 90° and a wind speed of $6\,m/s$, the torque is smaller in absolute value compared to hover. This means less power is required to drive the propeller.

The maximum measured pitching and yawing moment is approximately $0.08\,Nm$ or 66% of the sensor range in these directions. In contrast to small hub forces F_y and F_z compared to the thrust force F_x, the pitching moment M_y and yawing moment M_z can be of the same order of magnitude as the propeller torque M_x. The dimensionless moment coefficients in y and z direction are plotted in the second and third column of Fig. 8. C_{M_y} is positive at all propeller angles between 0° and 180°. Higher wind speed and propeller angles approaching 90° both enlarge this moment because of the increased difference in flow velocity through the disk. For a VTOL MAV operating its propellers near 90° propeller angle, this means the propellers tend to pitch up. The yawing moment coefficient C_{M_z} increases at higher wind speed and propeller angles near 90°. From helicopter disk theory as described in [20-22] and used in [17], this moment is explained by the higher lift force acting on the advancing propeller blade which experiences a higher air velocity compared to the retreating blade. In this experiment the propeller was turning counterclockwise, hence creating a negative moment around the z-axis. Because most VTOL MAVs use pairs of counter rotating propellers these relatively big moments, tending to roll the vehicle, cancel out each other but can bend the structure of the vehicle.

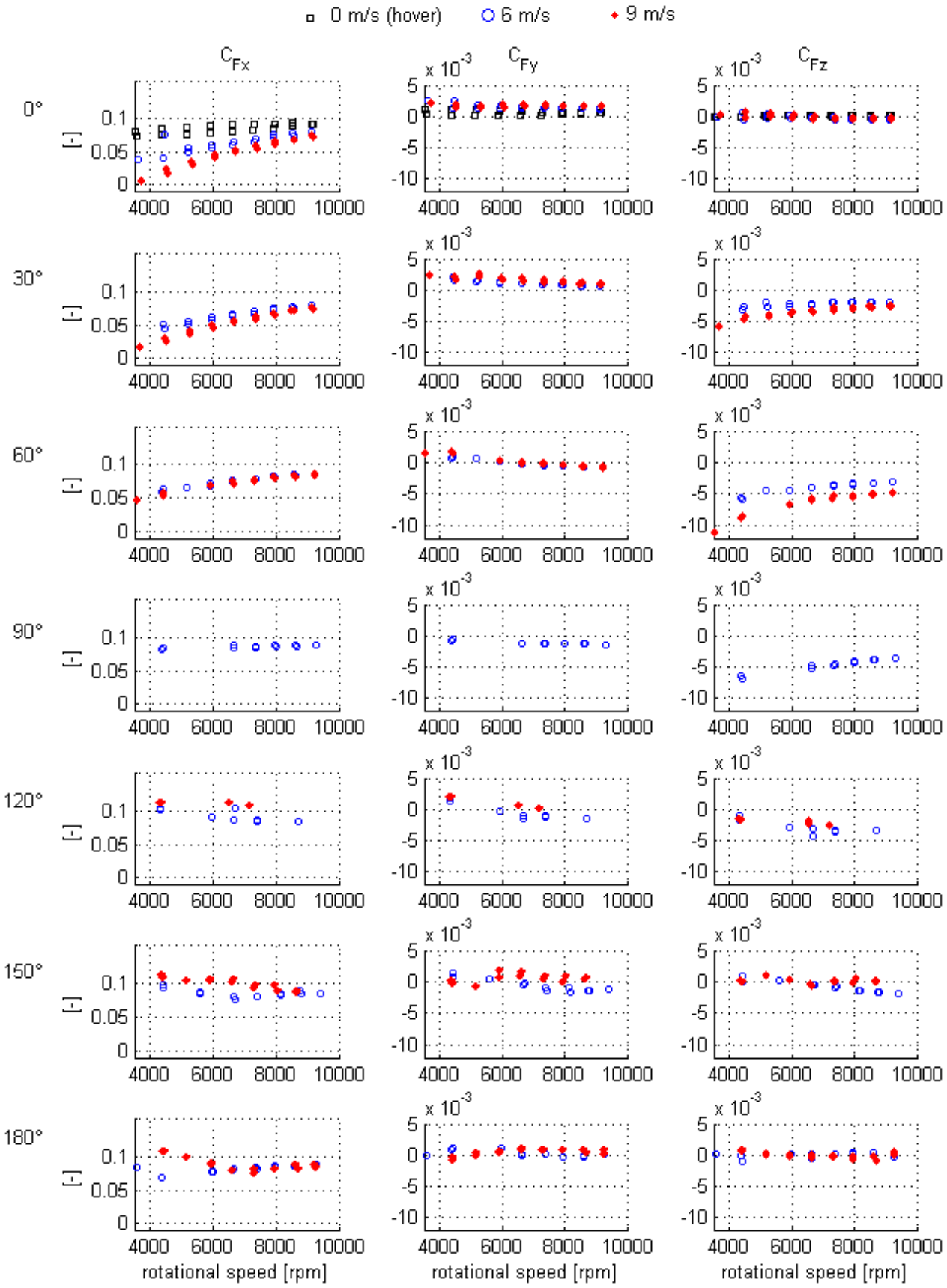

Figure 7. Dimensionless coefficients of the forces acting on a propeller in x, y and z direction for different wind speeds, propeller angles and propeller rotational speeds.

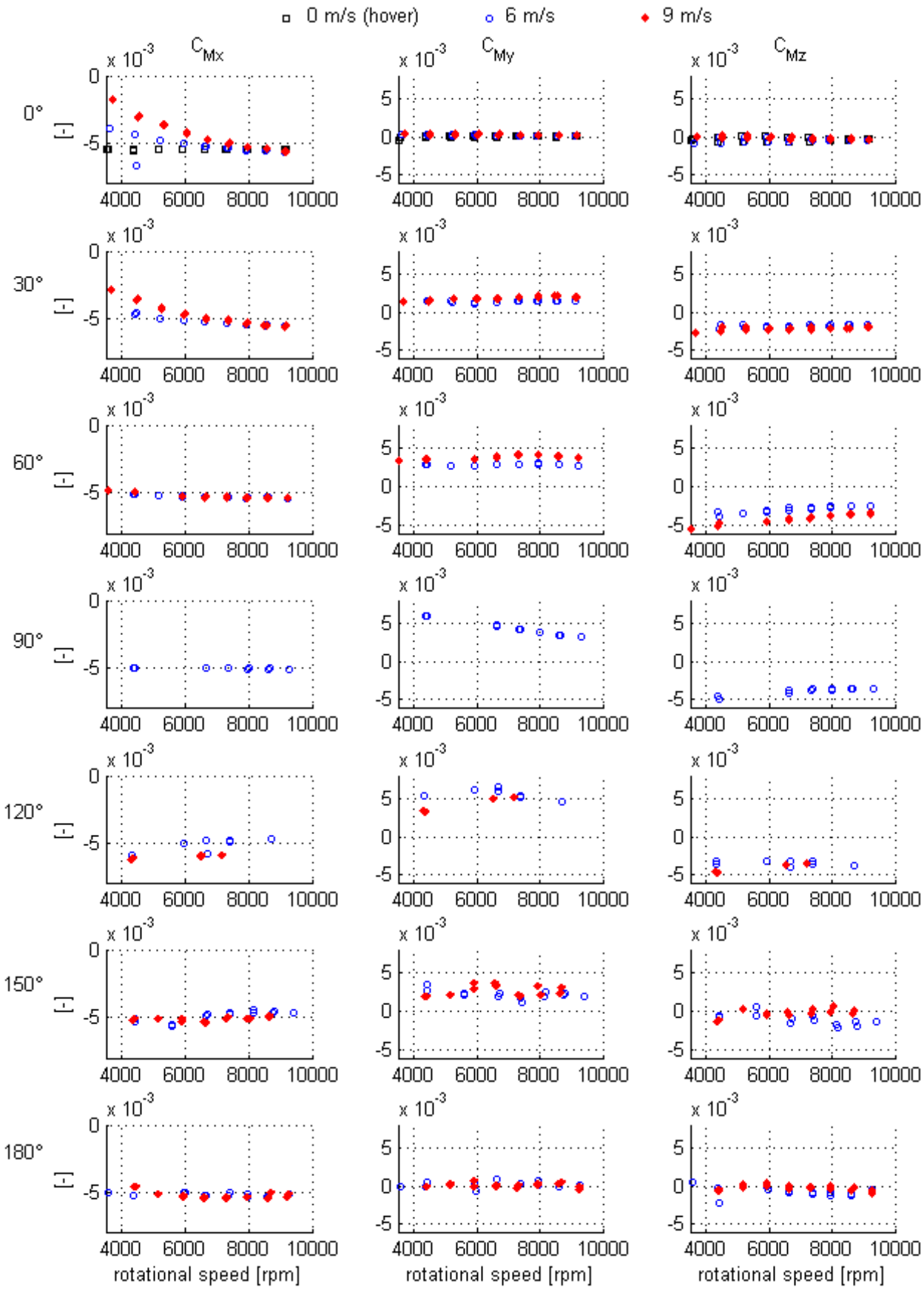

Figure 8. Dimensionless coefficients of the moments acting on a propeller in x, y and z direction for different wind speeds, propeller angles and propeller rotational speeds

4.4 Lift

Fig. 9 shows the relative difference in lift force on a propeller of a VTOL MAV flying at 6 m/s compared to lift force in hover condition. The lift force L is calculated as:

$$L = F_x \sin \alpha_{prop} - F_z \cos \alpha_{prop} \quad (3)$$

For several angles this relative difference is plotted for a range of mechanical powers required for the propeller. This graph shows that flying at 6 m/s and angles between 80° and 90°, representing a slow forward flight, results in an increased lift force for the same amount of mechanical power. So less power is required for the same amount of lift. This effect becomes smaller and disappears at higher power levels of the propeller.

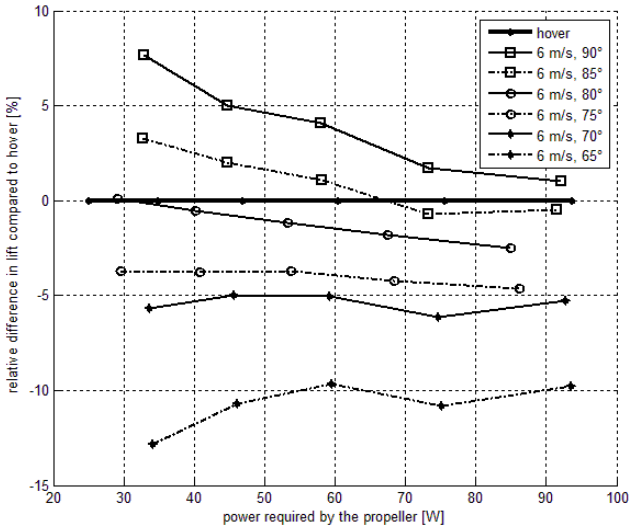

Figure 9. Relative lift difference of a VTOL MAV flying at 6 m/s compared to hover for several propeller angles.

4.5 ESC Efficiency

Fig. 9 shows the efficiency of the motor with ESC (2) for several rotational speeds at zero wind speed for two different experiments. In the first experiment, motor speed was controlled by changing the voltage of the power supply and keeping the throttle setting of the ESC at 100% , represented by the full line. The efficiency stays rather constant. The dashed line represents the efficiency calculated from a second experiment in which a constant voltage of 12 V is provided by the power supply and rpm is controlled by varying the throttle setting of the ESC. There is a dramatic decrease in efficiency with the ESC limiting the motor rpm. In an electric-powered MAV, the number of battery cells in series determines the supply voltage and maximum motor rpm. The ESC is used to limit the motor rpm in flight since supply voltage cannot be changed. To maximize efficiency of motor and ESC, battery voltage should not be chosen higher than needed to achieve the maximum desired rpm.

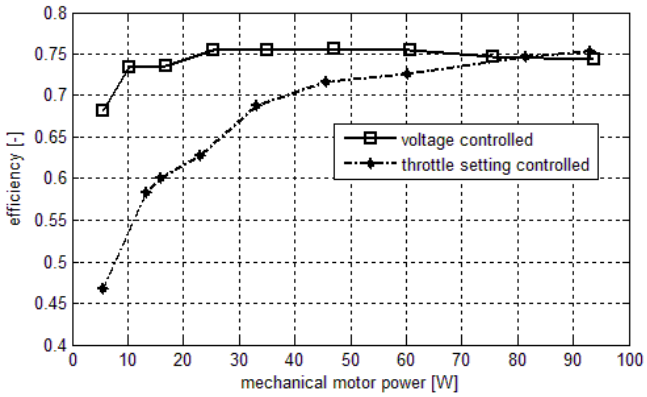

Figure 10. Efficiency of motor + ESC (electronic speed controller) combination as a function of the mechanical power for a voltage controlled and a throttle setting controlled case.

4.6 Frequency Analysis

Fig. 11 shows the frequency analysis of a measurement at zero wind speed and 9181 rpm (153 Hz). It shows that there are strong peaks in both forces and moments at certain frequencies. The first peak at 153 Hz on the graphs shows to be consistent with the measured propeller rotational speed hence spectral analysis can be a useful tool in measuring the propeller rotational speed. Vibrations were likely to be caused by imperfect balance of the propeller, small geometry differences between the two blades or inhomogeneous flow around the propeller. The latter is often the case for a propeller mounted on an arm of a multi-rotor VTOL MAV: the flow beneath the propeller is obstructed by the arm, so each time a propeller blade passes by, forces on the blade change, causing vibrations at two times the propeller rotational speed. Since the flow in this experiment is homogenous, no peak is expected at this frequency.

The frequency analysis in Fig. 12 is from the propeller turning 9297 rpm (155Hz) at 90° in a 6 m/s flow. Here peaks are visible at 310 Hz. The flow field is no longer homogenous, so each of the two blades experiences changing aerodynamic forces during each turn, resulting in force and moment oscillations at two times the rotational speed of the propeller.

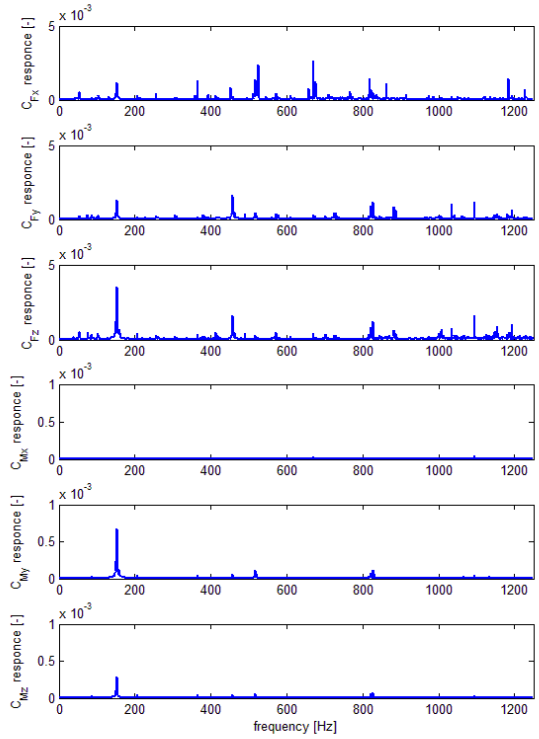

Figure 11. Frequency analysis of vibrations of the propeller turning 9181 rpm at zero wind speed.

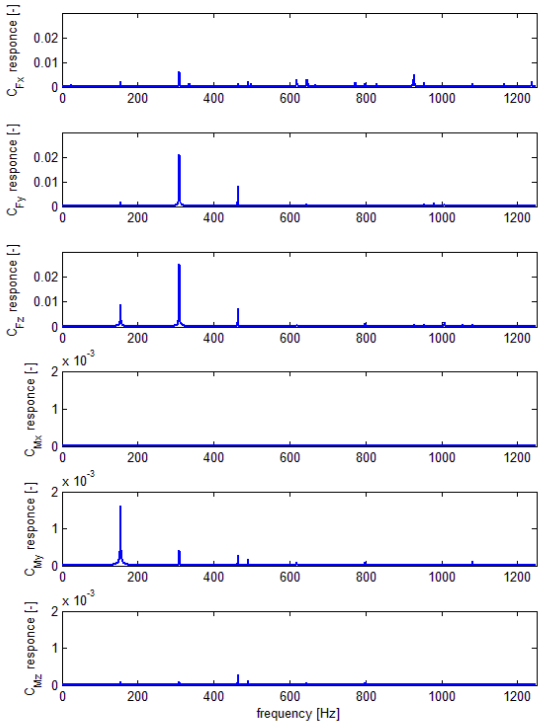

Figure 12. Frequency analysis of vibrations of the propeller turning 9297 rpm at 90° propeller angle and 6 m/s wind speed.

V. Conclusion

In contrast to other studies in which the air flow is parallel to the propeller shaft, this paper presents measured forces and moments acting on a propeller over its whole operating range. The thrust generation in descending flight of a VTOL MAV shows to cause unsteady descending behavior. Hub forces are very small compared to thrust force and mainly contribute to the vehicles drag. Flying at propeller angles between 90° and 80° at low power levels requires less power than needed during hover and can be used to extend the flight time. For these propeller angles, moments tend to flip the propeller backwards and rotate it around its z-axis. This pitching and yawing moment show to be of the same order of magnitude as the torque and therefore should not be neglected in design, modeling and control of VTOL MAVs. Additionally, efficiency calculations of motor and ESC combination reveal a decrease in efficiency up to 20% if motor power is limited by the ESC's throttle setting. This major efficiency loss must be taken into account in the design and modeling of an electrical powered MAV for deciding the battery voltage and ESC throttle setting.

Acknowledgment

The authors wish to thank Mathieu Torfs for his help with the wind tunnel setup and Jon Verbeke for his feedback on the results.

References

[1] O. Gur and A. Rosen, "Optimizing electric propulsion systems for unmanned aerial vehicles," in journal of Aircraft Vol. 46, No. 4,Technion – Israel Institute of Technology, Haifa 32000, Israel, July-August 2009.

[2] P.J. Bristeau, P. Martin, E. Salaün, N. Petit, "The role of propeller aerodynamics in the model of a quadrotor UAV," Proceedings of the European Control Conference 2009, Budapest, Hungary, August 2009.

[3] D. Griffiths and J. Leishman, "A study of dual-rotor interference and ground effect using a free-vortex wake model," in Proc. of the 58th Annual Forum of the American Helicopter Society, (Montréal, Canada), 2002.

[4] APC Advanced precision composites propeller dataset. [Online]. Available: http://www.apcprop.com/v/downloads/PERFILES_WEB/datalist.asp

[5] J. B Brandt and M. S. Selig. Propeller performance data at low Reynolds numbers. Technical report, University of Illinois, 2011.

[6] K. M. Asson and P. F. Dunn, "Compact dynamometer system that can accurately determine propeller performance," Journal of Aircraft, vol. 29, pp. 8-9, January-February 1992.

[7] Propeller database. [Online] Available: http://aerospace.illinois.edu/m-selig/props/propDB.html

[8] H. R. Hossain and Dr. N. Kroughlicof, "Propeller dynamometer for small unmanned aerial vehicle," Memorial University of Newfoundland, St. John's, NL, Canada.

[9] K. Kotwani, S. K. Sane, H. Arya, K. Sudhakar, "Experimental Characterization of propulsion system for mini aerial vehicle," 31st National Conference on FMFP, December 16-18, 2004, Jadavpur University, Kolkata.

[10] M. P. Merchant, “Propeller performance measurements for low Reynolds number unmanned aerial vehicle applications”, M.S. thesis, Wichita State University, Kansas, USA, 2004.
[11] H. S. Ribner, “Propellers in Yaw,” National Advisory Committee for Aeronautics, NACA Report No. 820
[12] R. E. Kuhn and J. W. Draper, “Investigation of the Aerodynamic Characteristics of a model wing-propeller combination and of the wing and propeller separately at angles of attack up to 90°,” NACA Report No. 1263
[13] H. S. Ribner, “Formulas for propellers in yaw and chards of the side-force derivative,” NACA Report No. 819
[14] P. B. S. Lissaman, “Low-Reynolds-Number Airfoils,” in Ann. Rev Fluid Mech. 1983. 15:223-39, AeroVironment Inc., Pasadena, California 91107.
[15] N. Guenard et al., “Control laws for the tele operation of an unmanned aerial vehicle known as an x4-flyer,” in Proc. (IEEE) International Conference on Intelligent Robots (IROS’06), Beijing, China, 2006.
[16] P. Pounds, R. Mahony, J. Gresham., “Towards Dynamically-Favourable Quad-Rotor Aerial Robots,” Australian National University, Canberra, Australia, 2004.
[17] G. M. Hoffmann et. Al., “Quadrotor Helicopter flight dynamics and control: theory and experiment,” AIAA Guidance, Navigation and Control Conference and Exhibit, South Carolina, August 2007.
[18] P. G. Dimitriadis. Aeroelasticity & experimental aerodynamics lab, University of Liege wind tunnel. [Online], Available: http://www.ltas-aea.ulg.ac.be
[19] Ati Industrial Automation [Online]. Available: https://www.ati-ia.com/
[20] W. Johnson, Helicopter Theory. Princeton, NJ: Princeton University Press, 1980.
[21] J. Leishman, “Principles of Helicopter Aerodynamics,” New York, NY: Cambridge University Press, 2000.
[22] R. Prouty, “Helicopter Performance, Stability, and Control,” Malabar, FL: Krieger Publishing Company Inc., 2003.
[23] O. R. Shetty and M. S. Selig, “Small-Scale Propellers Operating in the Vortex Ring State,” in 49th AIAA Aerospace Sciences Meeting 4.-7 January 2011, Orlando, FL, University of Illinois at Urbana-Champaign, Urbana, IL 61801, USA.